Development of High Efficiency Particulate Absorbing Filter Materials

Asis Patanaik,[1] Rajesh D. Anandjiwala,[1,2] Lydia Boguslavsky[1]

[1]*CSIR Materials Science and Manufacturing, Fibres and Textiles Competence Area, Port Elizabeth 6000, South Africa*
[2]*Department of Textile Science, Faculty of Science, Nelson Mandela Metropolitan University, Port Elizabeth 6031, South Africa*

Received 31 January 2009; accepted 15 March 2009
DOI 10.1002/app.30470
Published online 2 June 2009 in Wiley InterScience (www.interscience.wiley.com).

ABSTRACT: We have developed new high efficiency particulate absorbing filter materials by bonding the fiber web with the help of high pressure water jets emerging from micron sized nozzles and subsequently coating the filters with a chemical binder. Two different types of nonwoven filters are produced by varying the water jet pressure during the bonding process. The performance characteristics of the filter materials are evaluated in terms of filtration parameters, such as filtration efficiency, dust holding capacity, and pressure drop. Filtration efficiency depends on the pore characteristics, namely pore size and their distribution in the filters. The developed filter materials have shown promising performance characteristics by capturing higher amount of dust particles with a relatively low pressure drop during use. These filter materials can be used for a wide range of industrial applications, where high filtration efficiency is required at low energy consumption. A fluid flow simulation is carried out by computational fluid dynamics (CFD) to understand flow pattern during the bonding process. The CFD is also used to predict the pressure drop in the nonwoven filter materials during filtration process.
 J Appl Polym Sci 114: 275–280, 2009

Key words: fibers; modeling; structure

INTRODUCTION

Air filtration plays an important role in improving air quality and cleaner environment. The demands for better air quality increased greatly because of new regulations, new scientific knowledge, and a change in health consciousness. Nonwoven filter materials are the major media for dry and wet filtration applications. The distinctive porous structure of nonwoven fibrous assembly makes them ideal medium for the filtration application. Nonwoven materials are defined as fibrous structure made by bonding or interlocking fibers or filaments by mechanical, thermal, and chemical bonding or combination of these.[1]

The high efficiency particulate absorbing filter materials are designed to keep very small particles from entering a control environment or to prevent particles from escaping. These filter materials are excellent in removing high percentage of biological and particulate material from the air, with relatively low pressure drop and energy consumption.[2] The design consideration for the filter materials depends upon the properties of fibers, fiber arrangement, method of bonding the fibers, and extent of filtration required. Polypropylene fiber is selected for the development of high efficiency particulate absorbing filter materials because of their chemical inertness, low water absorption, and quick drying capacity which makes them ideal for such applications.

There is a lack of research work on the high efficiency particulate absorbing filters developed by water jets bonding or hydroentanglement (or spunlacing) bonding technique, which is an easy way to develop such type of filter materials. It is a mechanical method of bonding the nonwoven fibrous web with the help of high pressure water jets.[3,4] Other relevant literatures covering various aspects of hydroentanglement bonding technique can be found out from the literatures given in the references section.[5–10] A schematic representation of the hydroentanglement bonding process is shown in Figure 1. A series of high pressure columnar water jets is produced by pumping water through the cone capillary nozzles which are placed in a jet strip and clamped into the manifolds. These high velocity jets are directed to the fibrous web which is supported on a moving conveyer or perforated sheet. These jets exert enough force on the fibers to entangle them with each other, this result in the production of porous network of fibers. The perforated sheet being permeable, it enables most of the de-energized water to be drawn into suction or vacuum for recycling and reuse. Generally multiple manifolds are used to produce a well-bonded fabric.[11] Different range of water jet pressure is used in the different manifolds. The purpose of the first manifold is to prewet the

Correspondence to: A. Patanaik (patnaik_asis@yahoo.com).

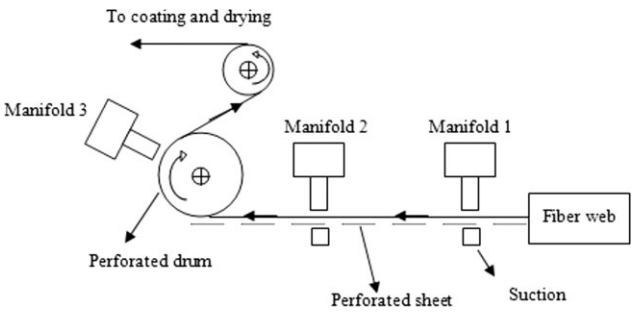

Figure 1 Schematic representation of the hydroentanglement process.

fibrous web, so a low pressure (10 bar) is maintained compared with the second and third manifolds. The second and third manifolds are used to bond the fibers with each other and generally a very high pressure in the range of 60-400 bar is applied. The selection of pressure range in the manifold depends upon requirement of the product for various functional applications and it is the most critical part of the whole process of hydroentanglement. A very high pressure would cause shifting of fibers which results in uneven structure and higher energy consumption. A very low pressure will result in poorly bonded fibrous assemblies which are not suitable for filtration applications. Based on our previous experience, two different pressure ranges are selected in different manifolds for developing high efficiency particulate absorbing filter materials. The performance characteristics of nonwoven filter material depend upon the arrangement of different pores. These pores are created due to different arrangement of fibers resulting from different jet pressures acting on them. When the jet pressure or the processing condition is varied during hydroentanglement bonding process, it may result in different structural arrangement of fibers in nonwoven materials, subsequently affecting the pore size and its distribution. So we have selected the pressure range that provides small pores which are needed for high efficiency particulate absorbing filter materials. Details of the pressure range are given in the experimental section.

Nonwovens are porous materials, so the pore characteristics need to be evaluated. The pore size and its distribution are measured on capillary flow porometer.[12] For the measurement of filtration parameters, ASHRAE standard 52.2 was adopted.[13] The dust filtration device was used to evaluate filtration efficiency, dust holding capacity, and pressure drop. Fluid flow and related phenomena can be described by computational fluid dynamics (CFD). Since reported studies in CFD are very few,[14–16] new CFD model needs to be developed for the better understanding of the hydroentanglement process. Similarly, CFD modeling in predicting the filtration efficiency by considering the pressure drop in the filter materials needs to be developed to have a realistic prediction of the filtration parameters. In the view of the preceding discussion, CFD models are developed for the hydroentanglement process and for predicting pressure drop during filtration process. CFD modeling was preformed by the software package Comsol Multiphysics.[17]

EXPERIMENTAL

Sample preparation

The nonwoven filter fabrics are produced by subjecting polypropylene fibers to carding, then orienting the carded web in the cross machine direction by using a cross lapper, subsequently subjecting it to the action of high pressure water jets. Three different levels of water jet pressure were selected in the manifolds for sample preparation. For sample S1 the jet pressures in bar were 10, 120, 120, and for S2, 10, 200, 200, for first, second, and third manifolds, respectively. Acrylate chemical binder of 25% concentration was applied over the filter material after the hydroentanglement process by foam bonding with traverse foam delivery mechanism technique and then filter materials are dried and cured at a temperature of 150°C in an oven. The binder used is an acrylic ester based acrylonitrile copolymer. The fineness and length of fibers utilized for sample preparation are 2.2 dtex and 40 mm, respectively.

Measurement of pore size and its distribution

The pore size and distribution were measured on a capillary flow porometer based on the principle of liquid extrusion porometry technique.[12] In this method, a wetting liquid with known surface tension of 15.9 dyne/cm spontaneously fills the pores of the specimen of 1 cm diameter, which is placed between two adapter plates in the sample holding chamber of the instrument. Air pressure is applied perpendicular to the plane of the saturated fabric to force out the liquid from it. This air pressure is applied in small incremental steps to gradually force out the liquid from the specimen, starting from largest pore which required the lowest air pressure, to the smallest pore, which require the highest air pressure. The diameter of the pore, D (μm) can be calculated from the flowing equation:

$$D = \frac{4\eta \cos\theta}{p} \tag{1}$$

where η is the surface tension of the wetting liquid (dyne/cm), p is the air pressure (dyne/cm^2), and θ is the contact angle (generally very small). The air pressure and airflow rate are used to represent a range of pore diameters.

TABLE I
Pore Size and Filtration Parameters of Nonwoven Materials

Sample code[a]	Water jet pressure (bar)	Pore diameter (μm)			Efficiency (%)	Dust holding capacity (g/m^2)	Pressure drop (Pa)	$R^{2\,b}$
		Smallest	Mean flow	Maximum				
S1	120	7.56	54.99	104.95	93.71	45.62	37.51	0.86
S2	200	6.91	28.54	65.16	99.43	74.40	25.0	0.80

[a] Thickness of S1 : 1.36 mm; S2 : 1.13 mm.
[b] R^2 is the correlation co-efficient between the average value of pressure measured from dust filtration device and average pressure drop in filters obtained from CFD.

Measurement of filtration parameters

The dust filtration apparatus was used to evaluate filtration parameters, namely filtration efficiency, dust holding capacity, and pressure drop according to ASHRAE standard 52.2.[13] Dust particles in the range of 0.6-180 μm are fed at a constant rate to the filtration device and deposited on the samples having an area of 0.0095 m^2.

RESULTS AND DISCUSSION

Pore size and filtration parameters of nonwoven filter materials

The results obtained from pore size and filtration test are summarized in Table I. The photographs of the filters along with images of the pores and fibers obtained at different pressures are shown in Figure 2.

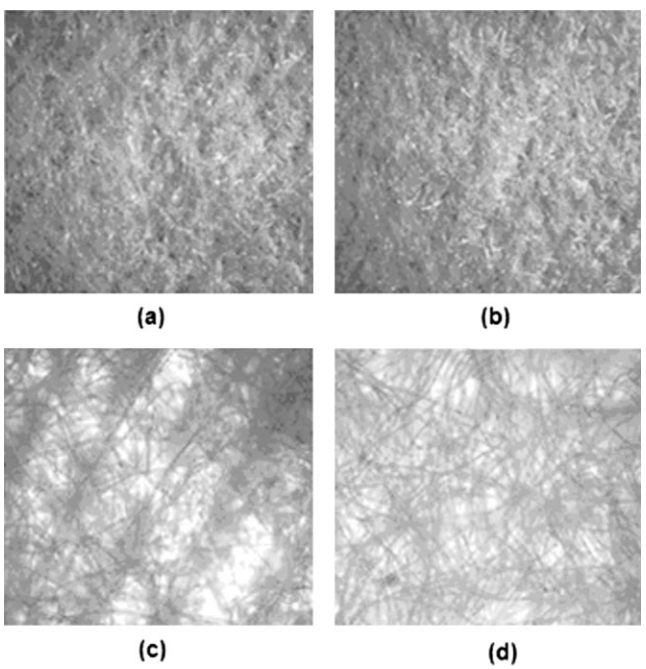

Figure 2 Photograph of high efficiency particulate absorbing filter material produced at different water jet pressure: (a) 120 bar and (b) 200 bar, magnification used is 10X. Corresponding images of the arrangement of pores and fibers in the filters obtained from a microscope: (c) 120 bar and (d) 200 bar, magnification used is 100 X.

There is no difference in the surface photographs obtained for both the filters produced at different pressures of 120 and 200 bar [Fig. 2(a,b)]. The microscopic images (100 x magnifications) of the two different filters show different arrangement of pores and fibers [Fig. 2(c,d)]. Filters that are produced at 120 bar pressure are comparatively open structure with larger pores in comparison to the one produced at 200 bar as evident from Figure 2(c,d). This may be because of the different degrees of entanglement tendency of the fibers depending upon the impact force of water jets acting on them. It may be expected that higher water jet pressure will create a more compact arrangement of fibers resulting in very small pores in filter materials in comparison with the one produced with low pressure, which is expected to be more porous material. The pore size distributions of nonwoven filter materials produced at different pressures is shown in Figure 3. In case of 120 bar water jet pressure, the pore size distribution follows a wider distribution in comparison with the 200 bar pressure which follows a narrow distribution. It may be because of the compact structure of the 200 bar pressure filter materials in comparison with the 120 bar as shown in Figure 3.

The important pore structure characteristics of nonwoven filter materials are the smallest pore diameter, the largest pore diameter, and the mean flow pore diameter.[18] The mean flow pore diameter is such that 50% of flow is through pores larger than the mean flow pore diameter and the rest of the flow is through smaller pores. Mean flow pore diameter is the

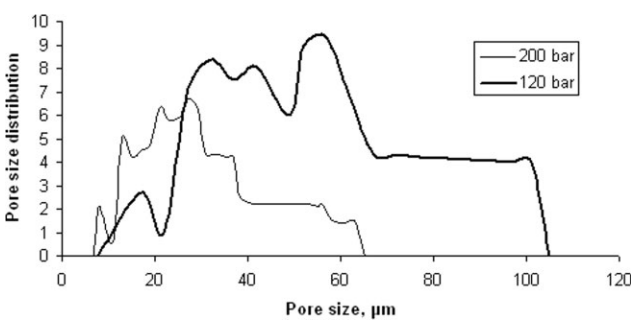

Figure 3 Pore size distribution of the filter materials produced at pressure levels of 120 and 200 bar.

diameter of the majority of the pores.[18–20] As the names suggest, the smallest and maximum pore diameters are the diameters of the smallest and largest pores, respectively. The pore sizes of nonwoven filter materials obtained from porometry is shown in Table I. There are decreases in smallest, maximum, and mean flow pore diameters as water jet pressure increases during hydroentanglement process. Generally, the filtration efficiency of a material is defined from the mean flow pore diameter. Because mean flow pore diameter decreases with the increase in water jet pressure, amount of dust particles passing through the filter is less and a larger amount of particles are now deposited on the filter. As a consequence of it, filtration efficiency is increased which is a measure of the amount of dust particles retained in the filter when introduced in the air stream. Also dust holding capacity increases and there is less pressure drop. Smallest and maximum pore diameters also decrease with the increase in water jet pressure. This is because of the greater entanglement of the fibers as a result of higher water jet pressure acting on them. It increases the frictional contact between the fibers and thereby covering the neighboring pores and decreasing the various types of pore sizes. With the increase in water jet pressure, there is also increase in the impact force acting on the fibers, which results in the greater entanglement of the fibers. Also coating the samples with the binder may further help in covering some pores. The pore characteristics namely pore size and its distributions play an important role in influencing filtration behavior.

Fluid flow simulation during hydroentanglement and filtration processes

The main part of the hydroentanglement bonding process is the cone capillary nozzle. A series of cone capillary nozzle is used to generate such high pressure water jets. A schematic representation of a typical cone capillary nozzle used for hydroentanglement process is shown in Figure 4(a). The specifications of the nozzle are: length (l) = 1 mm, inner diameter (d) = 0.12 mm, outer diameter (D) = 0.3 mm. These nozzles are generally arranged in a series in single or double row and placed on a long stainless steel strip of 1200 mm length, 25.4 mm width and 1 mm thickness. These strips run throughout the width of the machine and placed in the different manifolds. The distance between adjacent nozzles is about 500 μm. When very high pressure water suddenly enters the nozzle at 90° angle, constricted water jets are formed which are desirable for hydroentanglement process.[14,15] Constricted water jets are the flow inside the nozzle which is separated from the nozzle inner wall. Constricted water jets are always needed for creating well defined bonded fibrous structures. These

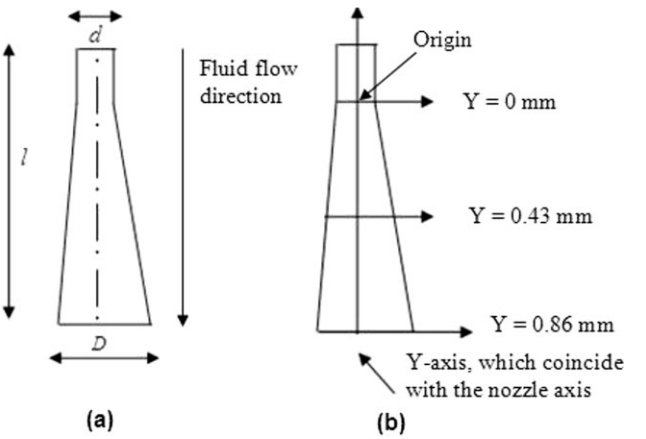

Figure 4 Schematic representation of a conical capillary nozzle (a) and (b) nozzle co-ordinate system.

constricted water jets give rise to a condition which allows the downstream air to flow inside the nozzle due to a pressure difference and envelop the water jet.[14,15] So the flow inside the nozzle is a mixture of two fluids i.e. water and vapor.

A three-dimensional (3D) fluid flow field inside the hydroentanglement nozzles was simulated. A schematic representation of the nozzle co-ordinate system for simulation purpose is shown in Figure 4(b). Fluid velocity profiles are measured at three different normal planes of nozzle. The throat of nozzle is considered as origin (x, y) = 0 as shown in Figure 4(b). This is the first section where velocity plots are taken. The second and third sections are at 0.43 mm and 0.86 mm, respectively, and plots are taken for velocity measurement. The fluid flow velocity in the hydroentanglement process was turbulent and hence the Re-Normalization Group (RNG) k-ε model of turbulence along with standard wall functions was used.[21] Pressure inlet and Pressure outlet boundary condition is used for the simulation purpose. At the wall no slip boundary condition is applied. A series of equations were used to solve an unsteady compressible turbulent flow of a mixture of water and vapor inside the nozzle. The Reynolds Averaged Navier-Stokes equation for a mixture of water and vapor can be given by[16,21]:
Mass conservation equation:

$$\frac{\partial(\rho_m)}{\partial t} + \frac{\partial(\rho_m u_{\mathrm{mi}})}{\partial x_i} = 0 \tag{2}$$

Momentum conservation equation:

$$\frac{\partial(\rho_m u_{\mathrm{mi}})}{\partial \mathrm{t}} + \frac{\partial}{\partial x_i}(\rho_m u_{\mathrm{mi}} u_{\mathrm{mj}}) = -\frac{\partial p}{\partial x_i} + \frac{\partial}{\partial x_j}\left[\mu\left(\frac{\partial u_{\mathrm{mi}}}{\partial x_j} + \frac{\partial u_{mj}}{\partial x_i} - \frac{2}{3}\delta_{\mathrm{ij}}\frac{\partial u_{\mathrm{ml}}}{\partial x_l}\right)\right] + \frac{\partial}{\partial x_j}(-\rho\overline{u'_{\mathrm{mi}}u'_{\mathrm{mj}}}) \tag{3}$$

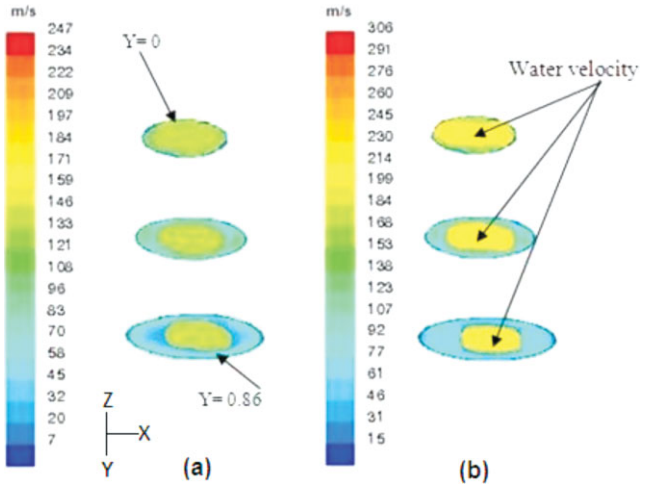

Figure 5 Velocity of water and vapor through a cone capillary nozzle at different pressure levels (a) 120 bar and (b) 200 bar. [Color figure can be viewed in the online issue, which is available at www.interscience.wiley.com.]

Turbulent kinetic equation:

$$\frac{\partial(\rho_m k)}{\partial t} + \frac{\partial(\rho_m k\, u_{\mathrm{mi}})}{\partial x_i} = \frac{\partial}{\partial x_j}\left[\left(\mu + \frac{\mu_t}{\sigma_k}\right)\frac{\partial k}{\partial x_j}\right] + G_m - \rho_m \varepsilon \tag{4}$$

Rate of dissipation of the turbulent kinetic energy:

$$\frac{\partial(\rho_{\mathrm{m}}\, \varepsilon)}{\partial t} + \frac{\partial(\rho_m\, \varepsilon\, u_{m\,\mathrm{i}})}{\partial x_i} = \frac{\partial}{\partial x_j}\left[\left(\mu + \frac{\mu_t}{\sigma_\varepsilon}\right)\frac{\partial \varepsilon}{\partial x_j}\right] + c_1 \frac{\varepsilon}{k} G_m - c_2 \rho_m \frac{\varepsilon^2}{k} \tag{5}$$

The nomenclature used is given below:
ρ_{m} = density of water and vapor mixture, t = time, u_m = velocity of water and vapor mixture, p = static pressure, u_{mi} = fluctuation in u_m in x-direction, $\rho\overline{u'_{\mathrm{mi}}u'_{\mathrm{mj}}}$ = Reynolds stress tensor, δ_{ij} = Kronecker's delta function, G_m = rate of generation of turbulent kinetic energy, k = turbulent kinetic energy, μ_t = turbulent viscosity, ε = rate of dissipation of turbulent kinetic energy and c_1, c_2, σ_k, σ_ε constants of the k-ε model.

The 3D-CFD results obtained from the water and vapor flow through a cone capillary nozzle at a pressure of 120 and 200 bar is shown in Figure 5. Y = 0 indicates a place close to the inlet of the nozzle and Y = 0.86 indicate the outlet of the nozzle. Each color in Figure 5 represents a particular velocity value in m/s, red being the highest and blue is the lowest. It can be seen from Figure 5 that water is flowing in a straight path with a constant velocity in the middle section of the nozzle, whereas the vapors are generated as a result of low pressure flow around the wall of the nozzle at a lower velocity. The average water velocity in the centre of the nozzle is around 159 m/s for 120 bar and 214 m/s for 200 bar as shown in Figure 5. With the increase in pressure, water velocity increases. The velocity of vapor is around 7 m/s and 15 m/s for 120 and 200 bar, respectively. These vapors may create some kind of recirculation effect in the nozzle. Since their velocity is very less in comparison with the water velocity, any kind of disturbance to the water flow stream can be neglected.

A nonwoven filter material model is created by considering the unit element i.e., the fiber, as a cylindrical rod.[22] The representation of fibers by a single element allows a significant reduction in computation time. The behavior of a single fiber can be combined and mapped onto the elements representing a bundle of fibers and ultimately representing these bundles of fibers in the nonwoven filter materials. The cylindrical rod element is assumed as a straight bar, loaded at its ends with uniform properties from end to end. This type of element has two degrees of freedom at each node, i.e., displacements in X- and Y- directions. In the nonwoven web structures, fibers are oriented in different directions, i.e., some fibers are in the machine direction, some fibers are in the cross-machine direction and other fibers do not have any preferential orientations or randomly oriented. In the modeling work, these three different fiber orientations are taken into account.

A 2D-simulation of pressure drop in the nonwoven filter materials during the filtration test is shown in Figure 6. The flow of steady state laminar incompressible air through the pores of nonwoven materials during the filtration process was simulated by solving the Navier-Stokes equation along with Darcy's law.[23–25] Pressure inlet and Pressure outlet boundary condition with no slip at wall are taken into account during the simulation purpose. The following equations (6–9) are used for pressure drop simulation.

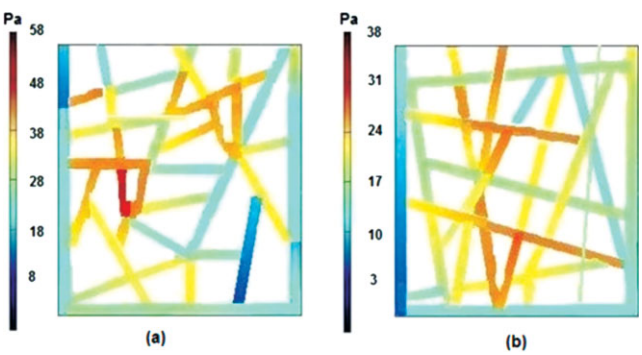

Figure 6 Pressure drop in the nonwoven filter materials (a) S1 and (b) S2. [Color figure can be viewed in the online issue, which is available at www.interscience.wiley.com.]

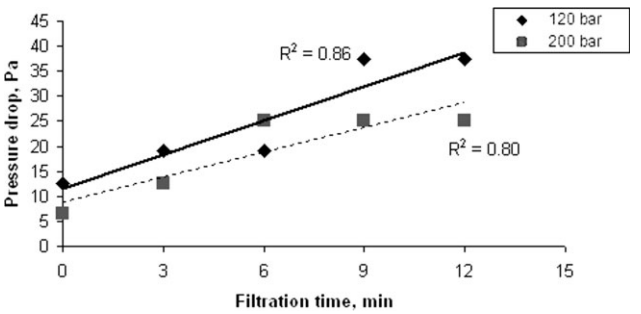

Figure 7 Pressure drop correlation between filtration test and CFD.

Mass conservation equation:

$$\nabla u = 0 \tag{6}$$

Momentum conservation equation:

$$\rho \frac{\partial u}{\partial t} - \nabla.[\mu(\nabla u + (\nabla u)^T)] + \rho(u\Delta)u + \Delta p = F \tag{7}$$

where, μ is the viscosity of air, ρ is the density of air, u is the velocity, p is the pressure, F is the force.

Darcy's law is given by:

$$\langle v \rangle = -\frac{1}{\mu} K \nabla \langle p \rangle \tag{8}$$

where ν is the velocity; μ is the viscosity; p is the pressure; and K is the permeability of the medium.

The pressure drop of a filter is a function of air viscosity (μ), filter thickness (t), face velocity (v), fiber diameter (d_f), and solid volume fraction (α).[26] It is given by:

$$\Delta p = \frac{\alpha \mu v t}{d_f^2} \tag{9}$$

Figure 6 is the top view of the simulated image of the nonwoven filter materials for pressure drop prediction. With the increase in water jet pressure, filtration parameters such as dust holding capacity increases with the decrease in pressure drop. Both the parameters indicate a very good particle absorbing filter materials with high efficiency and low pressure drop and energy consumptions. As discussed previously, with the increase in water jet pressure during hydroentanglement, structure of the filter will be more compact [Fig. 6(b)], so there will be less pressure drop compare with the structure which is produced at a lower water jet pressure as the web is more open [Fig. 6(a)]. As a consequence of it, there is a higher pressures drop for the later case (120 bar). There is a good correlation between the measured values of pressure drop from filtration test (shown by points) and from CFD (shown by lines) as observed in Figure 7 and Table I. So the developed nonwoven filter materials can be used as a high efficiency particulate absorbing filters for a wide range of applications.

CONCLUSIONS

The hydroentanglement or water jets bonding technique is used to develop new high efficiency particulate absorbing coated filter materials by varying the processing parameters. These filter materials have shown very high filtration efficiency (> 90%) in capturing dust particles in the range of 0.6–180 μm, accompanied with a relatively very low pressure drop during use. The pore size and its distribution play an important role in filtration characteristics. A CFD model is developed to simulate the fluid flow during the hydroentanglement process. It is also used for the prediction of pressure drop during the filtration process. The developed filters can be used for various industries, hospitals, and in homes where high degree of purity is required in the air.

References

1. Smith, P. A. In Handbook of Technical Textiles; Horrocks, A. R.; Anand, S. C., Eds; Woodhead Publishing Limited.: Cambridge, UK, 2000.
2. Curtis, L. Am J Infect Control 2007, 35, 138.
3. White, C. F. Tappi J 1990, 73, 187.
4. Connolly, T. J.; Parent, L. R. Tappi J 1993, 76, 135.
5. Berkalp, O. B.; Pourdeyhimi, B.; Seyam, A. Intl Nonwovens J 2003, 12, 28.
6. Ghassemieh, E.; Acar, M.; Versteeg, H. K. Compos Sci Tech 2001, 61, 1681.
7. Gilmore, T. F.; Timble, N. B.; Morton, G. P. Tappi J 1997, 80, 179.
8. Mao, N.; Russell, S. J. Compos Sci Tech 2006, 66, 80.
9. Pourmohammadi, A.; Russell, S. J.; Höffele, S. Text Res J 2003, 73, 503.
10. Seyam, A. M.; Shiffler, D. A.; Zheng, H. Intl Nonwovens J 2005, 14, 25.
11. Anand, S. C.; Brunnschweiler, D.; Swarbrick, G.; Russell, S. J. In Handbook of Nonwovens; Russell, S. J., Ed; Woodhead Publishing Ltd.: Cambridge, UK, 2007.
12. Capillary Flow Porometer, Instruction Manual, Porous Materials Inc.: Ithaca, New York, 2005.
13. ANSI/ASHRAE Standard 52.2. Method of Testing General Ventilation Air-Cleaning Devices for Removal Efficiency by Particle, 1999.
14. Tafreshi, H. V.; Pourdeyhimi, B. Exp Fluids 2003, 35, 364.
15. Tafreshi, H. V.; Pourdeyhimi, B. Text Res J 2004, 74, 359.
16. Anantharamaiah, N.; Tafreshi, H. V.; Pourdeyhimi, B. Chem Engg Sci 2006, 61, 4582.
17. Comsol Multiphysics 3.2, User Guide; 2005.
18. Jena, A.; Gupta, K. Intl Nonwovens J 2003, 12, 45.
19. Patanaik, A.; Anandjiwala, R. D.; Gonsalves, J.; Boguslavsky, L. Paper Presented in Finite Element Modeling of Textiles and Textile Composites Conference; St. Petersburg, Russia, September 26–28, 2007.
20. Mayer, E. Filtr News 2002, 20, 1.
21. Wilcox, D. C. Turbulence Modeling for CFD, 2nd ed.; Dcw Industries: California, 1998.
22. Patanaik, A.; Anandjiwala, R. D. J Appl Polym Sci 2008, 108, 3876.
23. Gresho, P. M.; Sani, R. L. Incompressible Flow and the Finite Element Method; John Wiley & Sons: New York, 2000; Vol. 1 and 2.
24. Darcy, H. Les Fontaines Publiques de la Ville de Dijon; Victor Dalmont Publication: Paris, 1856.
25. Patnaik, A.; Rengasamy, R. S.; Kothari, V. K.; Ghosh, A. Wetting and Wicking in Fibrous Materials; Textile Progress; Woodhead Publishing Ltd.: Cambridge, UK, 2006.
26. Rao, N.; Faghri, M. Aero Sci Tech 1988, 8, 133.